
Check for updates

(1)

where c and c_0 [mol/L] are, respectively, the concentration in the measured sample and at recharge, λ [T^{-1}] is the radionuclide decay constant and t_w [y] is the groundwater age. Estimates of groundwater age obtained with Eq. (1) are denoted as radiometric ages. It has been shown that in real systems, where mixing occurs as a results of dispersive fluxes, radiometric ages are biased toward younger ages and thus are also denoted as apparent ages (Cornaton et al., 2011). In fractured media, or in systems where thin conductive aquifers are confined by low permeability aquitards, diffusive mass exchange from the fracture/aquifer to the matrix/aquitard may also lead to biased estimates of groundwater age (Sudicky and Frind, 1981) and thus correction methods have been proposed (Neretnieks, 1981; Sanford, 1997). Varni and Carrera (1998) however showed that the mean groundwater age computed using the concept of conservation of groundwater age mass is not affected by matrix diffusion.

Besides radioisotopes, also stable naturally occurring isotopes can be used to date groundwater age (Bethke et al., 1999). The most common stable nuclide used for groundwater dating is indeed ^{4}He, which is produced by the alpha decay of radionuclides within the natural uranium and thorium decay series (Ballentine and Burnard, 2002). ^{4}He has been typically used to date groundwater age in porous aquifers (e.g. Torgersen, 1980; Torgersen and Clarke, 1985; Bethke et al., 1999). Under the assumption of a closed piston-like system, groundwater age can be estimated as:

$$t_w = \frac{\phi(c - c_0)}{R_\alpha} \tag{2}$$

where ϕ [-] is the aquifer porosity, R_α is the helium production rate [mol/m^3 y] and the other terms are as in Eq. (1).

In fractured media, the intact rock matrix might contain a certain amount of uranium and thorium (e.g. Trinchero et al., 2014 and references therein). Thus, helium generates in the matrix and back-diffuses into the adjacent water bearing fractures. It turns out that the use of linear accumulation methods to date groundwater age in fractured media is not trivial.

In this paper we present an analytical solution, which is a simple extension of linear accumulation methods, that allows ^{4}He data to be used for groundwater dating in fractured media. As in the classical version of the linear accumulation method (Eq. (2)), groundwater age is linearly dependent on ^{4}He concentration and inversely proportional to ^{4}He production rate. The latter term is however scaled here by the inverse of fracture volume fraction (i.e. the fracture volume divided by the bulk volume of medium). This scaling term provides the link with the underlying matrix diffusion processes. The proposed solution is validated using a simple test case. In the second part of the paper, we provide a formulation for the numerical simulation of steady-state ^{4}He levels in fractured media. The formulation is based on an Equivalent Continuous Porous Medium (ECPM) conceptualisation of the fractured system and is used here to further validate the proposed analytical solution.

2. Problem formulation

In sparsely fractured rock, groundwater typically flows along complex networks of fractures (Fig. 1 left). Through simplification, this otherwise incredibly complex system is often conceptualised as a network of quasi-parallel flow pathways ((e.g. Sudicky and Frind, 1982); see Fig. 1 right). Under this hypothesis, transport of a long-lived non-sorbing nuclide is described by these two coupled partial differential equations:

$$\frac{\partial c_f}{\partial t} + v\frac{\partial c_f}{\partial x} - D_L\frac{\partial^2 c_f}{\partial x^2} = \frac{\phi D_p}{\delta_f}\frac{\partial c_m}{\partial z}\bigg|_{z=0}$$

and

$$\frac{\partial c_m}{\partial t} = D_p\frac{\partial^2 c_m}{\partial z^2} + F \qquad 0 \leqslant z \leqslant \delta_m \tag{4}$$

where c [mol/m^3_w] is the concentration of radionuclide in solution (from hereafter, subscripts m, f and w are used to refer to the rock *matrix*, the *fracture* and the *water*, respectively), v [m/y] is the water velocity in the fracture, ϕ [–] is the rock matrix porosity, D_p [m^2/y] is the pore diffusion coefficient in the matrix, δ_f [m] is half of the fracture aperture, $1/\delta_f$ [m^{-1}] is the fracture specific surface area and F [mol/m^3_w· y] is the radionuclide production rate in the matrix. Hydrodynamic dispersion, D_L [m^2/y], is expressed as

$$D_L = \alpha_L v + D_w \tag{5}$$

where α_L [m] is the longitudinal dispersivity and D_w [m^2/y] is the diffusion coefficient in unconstrained solution.

For the sake of convenience, the origin of the z-axis is placed at the matrix/fracture interface and not in the middle of the fracture.

The following boundary conditions apply.

$$c_f(0, t) = 0 \tag{6a}$$

$$c_m(x, 0, t) = c_f(x, t) \tag{6b}$$

$$\frac{\partial c_m}{\partial z}(x, \delta_m, t) = 0 \tag{6c}$$

where δ_m [m] is the available matrix extent, which is typically assimilated to the average fracture half-spacing. We will discuss later about different boundary conditions to be applied at the outlet boundary ($x = L$).

Note that this problem formulation mimics the infiltration of nuclide-free water and the production of a nuclide in the rock matrix. Thus, this set of equations is suited to simulate transport of radiogenically produced ^{4}He, which is produced by the alpha decay of radionuclides within the natural uranium and thorium decay series.

At steady state, Eq. (4) has the following solution

$$c_m(x, z) = c_f(x) + \frac{Fz}{2D_p}(2\delta_m - z) \tag{6d}$$

and the fracture/matrix interfacial surface flux is

$$\phi D_p\frac{dc_m}{dz}\bigg|_{z=0} = \phi F\delta_m \tag{6e}$$

At steady state, the transport equation in the fracture (Eq. (3)) can conveniently be re-written in terms of dimensionless distance ($\theta = x/L$) and Peclet number ($Pe = vL/D_L$)

$$\frac{1}{Pe}\frac{d^2c_f}{d\theta^2} - \frac{dc_f}{d\theta} + \frac{L}{\delta_f v}(F\phi\delta_m) = 0 \qquad 0 \leqslant \theta \leqslant 1 \tag{6f}$$

For the outlet boundary ($\theta = 1$), we consider here two alternative boundary conditions

$$c_f = 0 \tag{10a}$$

or

$$\frac{dc_f}{dx} = 0 \tag{10b}$$

Eq. (10a) (i.e., a Dirichlet boundary condition) could be used to simulate e.g. rapid ^{4}He degassing at the outlet, while Eq. (10b) (Neumann boundary condition) could mimic advective discharge in conductive quaternary sediments. It is worthwhile noting that, for mathematical convenience, most of the available analytical solutions for transport in fractured rock assume instead a semi-infinite domain.

The solution of Eq. (6f) is

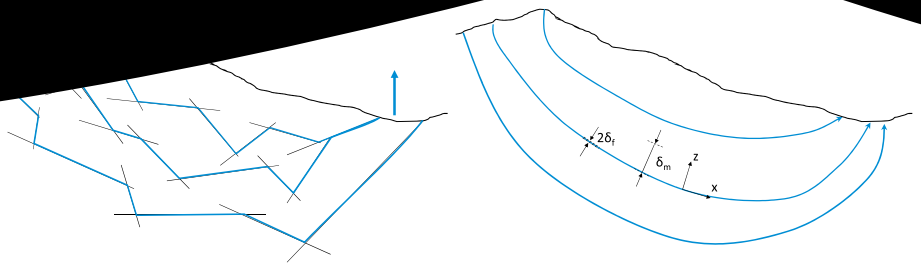

Fig. 1. (left) Idealised sketch showing flow pathways in a fractured medium and (right) simplified conceptualisation used in this work. Downward and upward arrows indicate water recharge and discharge, respectively. Parameters used in the mathematical formulation are also indicated: half of fracture aperture (δ_f [m]) and half of fracture spacing (δ_m [m]).

Table 1
Parameters of the validation problem.

Symbol	Quantity	Value	Unit
δ_f	Half fracture aperture	2.5×10^{-4}	m
δ_m	Half fracture spacing	1.0×10^{-1}	m
L	Fracture length	0.5	m
ϕ	Matrix porosity	1.0×10^{-3}	–
$\|\|\boldsymbol{q}\|\|$	Fracture water volumetric flux	3.1×10^{-1}	m/y
D_w	Diffusion coefficient in unconstrained solution	3.1×10^{-2}	m^2/y
D_p	Pore diffusion coefficient	3.1×10^{-3}	m^2/y
G	^{4}He bulk production rate in matrix	1.2×10^{-10}	mol/m^3 y

$$c_f = \eta\left(\frac{\exp(Pe\theta) + \theta(1-\exp(Pe)) - 1}{1-\exp(Pe)}\right) \tag{11}$$

for the Dirichlet boundary condition and

$$c_f = \eta\left(\theta + \frac{\exp(-Pe) - \exp((\theta-1)Pe)}{Pe}\right) \tag{12}$$

for the Neumann boundary condition, where

$$\eta = \frac{L}{v\delta_f}(F\phi\delta_m) = \frac{t_w(L)}{\delta_f}(F\phi\delta_m) \tag{13}$$

It is interesting to note that $t_w(L)$ in Eq. (13) is the groundwater residence time at the pathway outlet. This term has been used synonymously with the term *groundwater age* (Bethke and Johnson, 2008). Groundwater age at given positions along the pathway can then be written as

$$t_w(\theta) = \frac{c_f}{G}\frac{\delta_f}{\delta_m}\theta\left(\frac{\exp(Pe\theta) + \theta(1-\exp(Pe)) - 1}{1-\exp(Pe)}\right)^{-1} \tag{14}$$

for the Dirichlet boundary condition and

$$t_w(\theta) = \frac{c_f}{G}\frac{\delta_f}{\delta_m}\theta\left(\theta + \frac{\exp(-Pe) - \exp((\theta-1)Pe)}{Pe}\right)^{-1} \tag{15}$$

for the Neumann boundary conditions. Here $G = F\phi$ [mol/m^3· y] is the bulk production rate of ^{4}He in the rock matrix.

For high Peclet numbers, Eq. (12) reduces to

$$c_f = \eta\theta \tag{16}$$

and groundwater age simplifies to

$$t_w(\theta) = \frac{c_f}{G}\frac{\delta_f}{\delta_m} \approx \frac{c_f}{G}\omega_f \tag{17}$$

where ω_f [–] is the fracture volume fraction (note that the approximation is valid as long as fracture aperture is much smaller than fracture spacing).

Based on site characterisation studies conducted in three Fennoscandian fractured crystalline media (Olkiluoto in Finland and Forsmark and Laxemar in Sweden; (Drake et al., 2006; Eichinger et al., 2006)), Trinchero et al. (2014) showed that the ^{4}He production rate in the matrix of these three fractured media is well known and relatively constant: $G = 1.1 - 1.4{\cdot}10^{-10}$ mol/(m^3 y). We will use a value of $1.2{\cdot}10^{-10}$ mol/(m^3 y) in the calculations hereafter.

It is interesting to note that Eq. (17) is formally identical to the equation typically used in linear accumulation methods to date groundwater age in sedimentary porous aquifers using ^{4}He data (Eq. (2)). The only difference here is that the production rate is scaled by the inverse of the fracture volume fraction, which provides a direct link with the underlying mass exchange processes between the rock matrix and fractures.

3. Model validation

A simple problem, based on a system including a rock matrix and a single planar fracture, is solved numerically to validate the analytical solutions developed in the previous section. The parameters of the problem are summarised in Table 1. The numerical calculations were carried out using the numerical code PFLOTRAN (Lichtner et al., 2013; Hammond et al., 2014). The PFLOTRAN model was discretised with a structured grid and with constant refinement in the direction parallel to flow, using 500 grid cells, whereas 750 cells were employed in the perpendicular direction (with the first 250 cells having a size of $5{\cdot}10^{-6}$ m and the remaining 500 cells, located further away from the fracture, with a refinement of $2{\cdot}10^{-4}$ m) with a total of 375, 000 grid cells. Two calculation cases were performed, the first with longitudinal dispersivity set to $\alpha_L = 0.1$ m ($Pe = 2.5$) and the second with $\alpha_L = 0.05$ m ($Pe = 3.3$). All the calculations were carried out in the JURECA booster module (Jülich Supercomputing Centre, 2018). The results of the validation exercise are shown in Fig. 2. The analytical solutions of Eq. (11) (Dirichlet boundary condition) and 12 (Neumann boundary condition) agree well with the numerical calculations. With the low Peclet numbers considered here, Eq. (16) provides a reasonable approximation to Eq. (12) only relatively far from the outlet boundary. The divergence between the full analytical solution (Eq. (12)) and its simplified formulation (Eq. (16)) has implications for the groundwater dating technique proposed here, as it can lead to lower estimates of groundwater age close to the outlet boundary, particularly at low Peclet numbers.

From the set of equations presented in the previous section, it is evident that the transport in the fracture can be decoupled from the matrix at steady state by including Eq. (6e) into Eq. (3). The related differential equation can then be written as follows

$$v\frac{dc_f}{dx} - D_L\frac{d^2c_f}{dx^2} = \Gamma \qquad 0 \leqslant x \leqslant L \tag{18}$$

where $\Gamma = G(\delta_m/\delta_f) \approx G/\omega_f$ [mol/(m^3 y)] is the scaled ^{4}He production rate.

The validation of the analytical solution has here been repeated, only for the case of $Pe = 2.5$, using this formulation; i.e. transport has

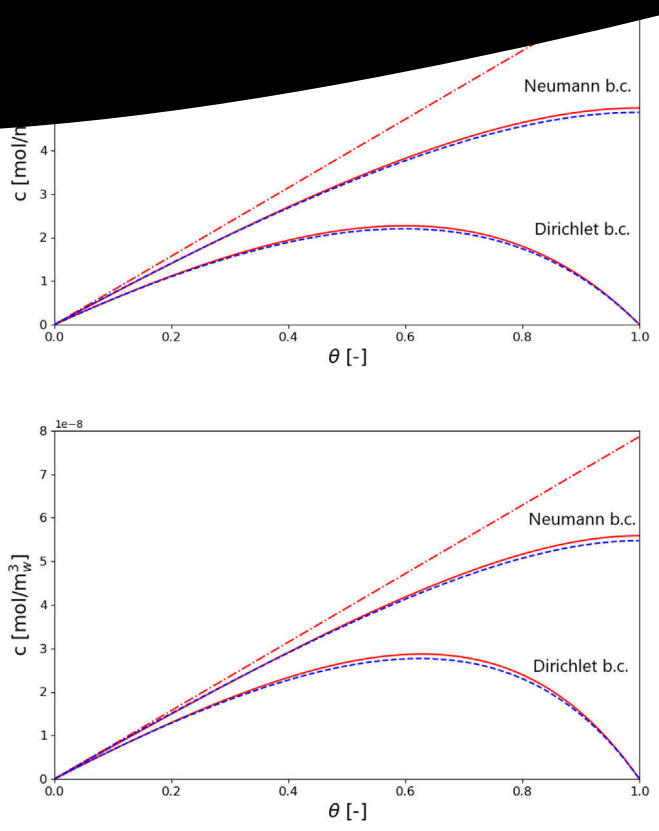

Fig. 2. ^{4}He concentration along the flowing fracture computed using the Dirichlet and the Neumann boundary conditions for (top) $Pe = 2.5$ and (bottom) $Pe = 3.3$. The blue dashed lines are the results of the PFLOTRAN simulations while the red continuous lines are the two analytical solutions (Eqs. (11) and (12)). The dashed dotted line is the analytical solution for an infinite Peclet number (Eq. (16)). Distance is normalised by the total fracture length ($\theta = x/L$).

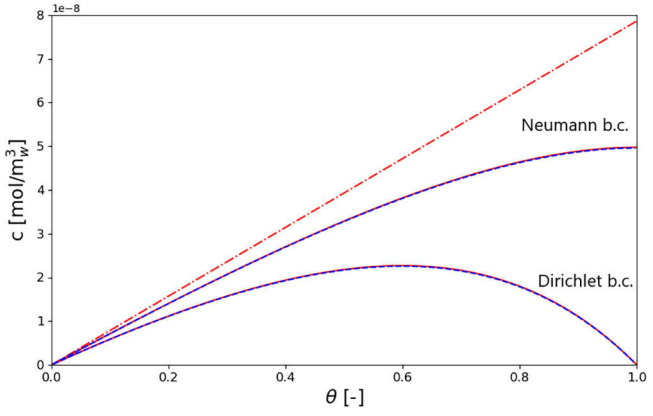

Fig. 3. ^{4}He concentration along the flowing fracture computed using the Dirichlet and the Neumann boundary conditions for $Pe = 2.5$. The blue dashed lines are the results of the PFLOTRAN 1D calculations while the red countinuous lines are the two analytical solutions (Eqs. (11) and (12)). The dashed dotted line is the analytical solution for an infinite Peclet number (Eq. (16)). Distance is normalised by the total fracture length ($\theta = x/L$).

ived using a PFLOTRAN
lidation are shown in Fig. 3.

4. Continuum-based formulation

Continuum models, based on Equivalent Continuous Porous Media (ECPM) conceptualisations of the fractured systems, have been long identified as appealing and numerically efficient tools to investigate groundwater flow and transport in fractured media (Neuman, 1988; Selroos et al., 2002; Trinchero et al., 2017; Iraola et al., 2019). In these types of models, an underlying Discrete Fracture Network (DFN) is used to derive equivalent parameters for the Equivalent Continuous Porous (ECP) medium. Among the different available upscaling methodologies (e.g. SKB, 2011 and references therein), the geometrical approach, in which intersecting volumes between fractures and grid cell control volumes are computed, and contributions from all intersecting fractures are added to the related parameters (Svensson, 2001; Svensson, 2001; Hadgu et al., 2017), is probably the most commonly used. More specifically, in this approach the contribution of each fracture to the permeability tensor is computed using some empirical relationship (typically, the cubic law (Witherspoon et al., 1980)) while kinematic porosity (Φ) is equivalent to the fracture volume fraction, ω_f. Using this approach, the steady-state distribution of ^{4}He concentration can be simulated using the following formulation

$$\nabla\cdot(\boldsymbol{q}c - \boldsymbol{D}\nabla c) = G \tag{19}$$

where $\boldsymbol{q}$ [m/y] is the Darcy flux vector, $\boldsymbol{D} = \alpha\boldsymbol{q}$ [m^2/y] is the dispersion tensor and α [m] is the isotropic dispersivity value. It is interesting to note that G in Eq. (19) is the bulk ^{4}He production rate in the rock matrix which is no longer scaled by the fracture volume fraction, as opposed to Eq. (18). In fact, Eq. (18) is valid for a single fracture, whereas Eq. (19) is valid for a generic three-dimensional DFN-derived ECPM model.

4.1. Test Case #1 (TC1)

An illustrative example is here used as a demonstrative problem for the proposed continuum-based formulation. The problem considers a 2D vertical cross section of a sparsely fractured bedrock (SFB) with a size of 964 m × 128 m. Flow and transport are mostly channeled along two highly transmissive deformation zones (DZ's) (see Fig. 4). The SFB is assumed to have a permeability $k^{SFB} = 1{\cdot}10^{-18}$ m^2 and a fracture volume fraction $\omega_f^{SFB} = 1{\cdot}10^{-4}$, whereas the DZ's have higher permeability and fracture volume fraction, due to the higher fracture intensity ($k^{DZ} = 1{\cdot}10^{-14}$ m^2 and $\omega_f^{DZ} = 1{\cdot}10^{-2}$). Inlet and outlet boundaries are located at coordinates (0:10;128) and (954:964;128), respectively and the domain was discretised using $241 \times 64 = 15{,}424$ regular grid cells (4 m × 2 m). A pressure difference $p_{in} - p_{out} = 10,000$ Pa is applied between the inlet and the outlet. The transport model includes three solutes: ^{4}He, a conservative tracer and groundwater age. Zero ^{4}He concentration and unitary concentration of the conservative tracer are prescribed at the inlet boundary. Consistently with the framework of Goode (1996), groundwater age is subject to the same transport equation and related processes used to simulate the transport of the conservative tracer, with the only difference that a zero-order source term accounts for aging. Groundwater age, and therefore also the age mass flux, is set to zero at the inlet boundary. The initial concentration is set to zero for the three species and a boundary condition of no dispersion across the outlet is prescribed. The calculations were carried out using PFLOTRAN, with dispersivity being set to 1 m. The simulation time frame is long enough so that ^{4}He and mean groundwater age have attained steady state. It is worthwhile noting that no matrix diffusion is included in the calculation. This implies that the transient analysis of the transport of the conservative solute that is presented hereafter is only intended to provide a description of groundwater flow patterns. Both mean groundwater age (i.e. Goode's equation) and ^{4}He are instead analysed at steady state. As shown by Varni and Carrera (1998), mean

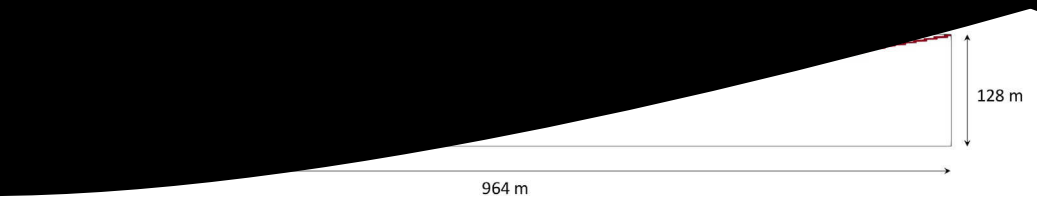

Fig. 4. cells are two … rest of the (hidden) … fractured bedrock (SFB).

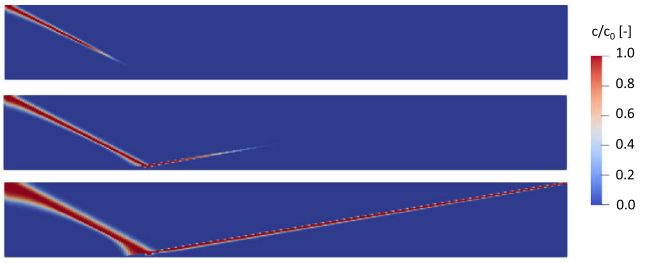

Fig. 5. TC1: tracer concentration at time (top) 1000 y, (middle) 2000 y and (bottom) 5000 y. Concentration values are normalised by the concentration in the boundary water.

groundwater age is not affected by matrix diffusion. So, it is consistent to compare estimates of mean groundwater age with corresponding estimates obtained using ^{4}He concentration and Eq. (17) (note also that, at steady state, the influence of matrix exchange processes on ^{4}He levels is accounted for by means of the production term, as discussed in Section 4 above).

Three different time snapshots of tracer concentration are shown in Fig. 5. As expected, relatively quick tracer penetration is observed along the DZ's whereas advection through the SFB is much slower. ^{4}He concentrations are analysed at 100,000 y (at this time ^{4}He levels are already at steady state). ^{4}He levels follow similar but inverted patterns as the tracer (Fig. 6), with lower concentration values observed along the two deformation zones, due to the effect of infiltrating water, and higher concentration values observed in the SFB, where the effect of in situ production of ^{4}He in the matrix is significantly stronger than the effect of infiltration of helium-free water.

The ^{4}He concentration values can be used to date groundwater age using Eq. (17). It is worthwhile noting that, when applied to a continuum model, the proposed mathematical expression depends on the spatial distribution of fracture volume fraction. Thus, similarly to what already observed by Varni and Carrera (1998) for kinematic age estimates, in heterogeneous media the solution does not provide a continuous distribution of groundwater age. To qualitatively validate the proposed framework, the results of groundwater age computed using ^{4}He data are compared with estimates of mean groundwater age (Goode, 1996), which instead provide a continuous distribution. The comparison between the two sets of results is shown in Fig. 7. Due to the linear relationship between ^{4}He derived groundwater age and fracture volume fraction, estimates along the deformation zones tend to be higher than corresponding estimates from groundwater age mass, whereas significantly lower values are observed in cells located outside but nearby the deformation zone. These cells are characterised by lower fracture volume fraction and relatively low ^{4}He content. This effect is

Fig. 6. TC1: ^{4}He concentration at steady state. Maximum computed ^{4}He concentration is $1.2{\cdot}10^{-2}$ mol/m^3_w.

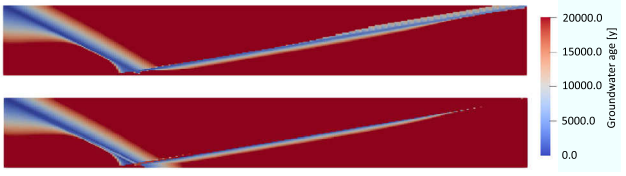

Fig. 7. TC1: groundwater age as computed (top) explicitly solving the equation of conservation of groundwater age mass (Goode, 1996) and (bottom) using Eq. (17).

further amplified when dispersive fluxes are increased by e.g. using higher dispersivity values (results are not shown here). Despite these differences, the generally good agreement between the two set of results points out that the proposed analytical solution (Eq. (17)) can be used to obtain approximated values of groundwater age in fractured media.

4.2. Test Case #2 (TC2)

A second, more realistic, test case is presented here. TC2 is loosely based on a groundwater flow model for Laxemar, Sweden (Vidstrand et al., 2010). Laxemar was one of the two sites that were thoroughly characterised during the siting process for a spent nuclear fuel repository in Sweden (the second site, Forsmark, was finally selected as the candidate site for the proposed repository).

The sparsely fractured rock was simulated using a Discrete Fracture Network that was generated using DarcyTools (Svensson and Follin, 2010; Svensson and Ferry, 2014). In DarcyTools the generation of stochastic fractures is governed by the following equation:

$$n = \frac{I}{a}\left[\left(\frac{l + dl}{l_{ref}}\right)^{a} - \left(\frac{l}{l_{ref}}\right)^{a}\right] \tag{20}$$

where n is the number of fractures per unit volume, I [m^{-3}] is the intensity, a [–] is the power law exponent and l_{ref} [m] is the reference length, which was set to 1 m here.

Fracture orientation follows a Fisher distribution characterised by the following parameters:

$$\lambda_1 = \cos(90 - tr)\cos(pl)\kappa \tag{21a}$$

$$\lambda_2 = \sin(90 - tr)\cos(pl)\kappa \tag{21b}$$

$$\lambda_3 = -\sin(pl)\kappa \tag{21c}$$

where tr and pl are the mean trend and mean plunge, respectively, and κ is the Fisher concentration.

The following power-law relationship between fracture transmissivity (T_f [m^2/s]) and fracture size (l [m]) is considered:

$$\log(T_f) = \log\left[a_T\left(\frac{l}{100}\right)^{b_T}\right] + d_T U[-0.5, 0.5] \tag{22}$$

where a_T [m^2/s] is the transmissivity of a fracture of size $l = 100$ m and b_T [–] is the power-law exponent. U is the uniform distribution and d_T [–] is a scaling factor.

The parameters of the model were taken from the shallow part of the Hydraulic Rock Domain (HRD) at Laxemar (Vidstrand et al., 2010) and are summarised in Tables 2 and 3.

				Set 4
		15–1000		
	$5.0 \cdot 10^{-2}$	$8.0 \cdot 10^{-2}$	$6.1 \cdot 10^{-2}$	$1.3 \cdot 10^{-1}$
Aperture [m]		$1.0 \cdot 10^{-4}$		
Power law exponent a [–]	-2.6	-2.5	−2.7	−2.7
λ_1 [–]	4.0	−4.9	−7.7	0.8
λ_2 [–]	−8.7	−11.0	0.02	0.8
λ_3 [–]	−0.6	−0.3	−1.1	−12.0

Table 3
Coefficients of the power-law function used to generate fracture transmissivity in Test Case #2 (Eq. (22)).

Parameter	Set 1	Set 2	Set 3	Set 4
a_T [m^2/s]	$4.5 \cdot 10^{-7}$	$2.2 \cdot 10^{-6}$	$2.2 \cdot 10^{-6}$	$2.5 \cdot 10^{-6}$
b_T [–]	0.5	0.6	0.6	0.7
d_T [–]	0.8	1.4	1.0	1.4

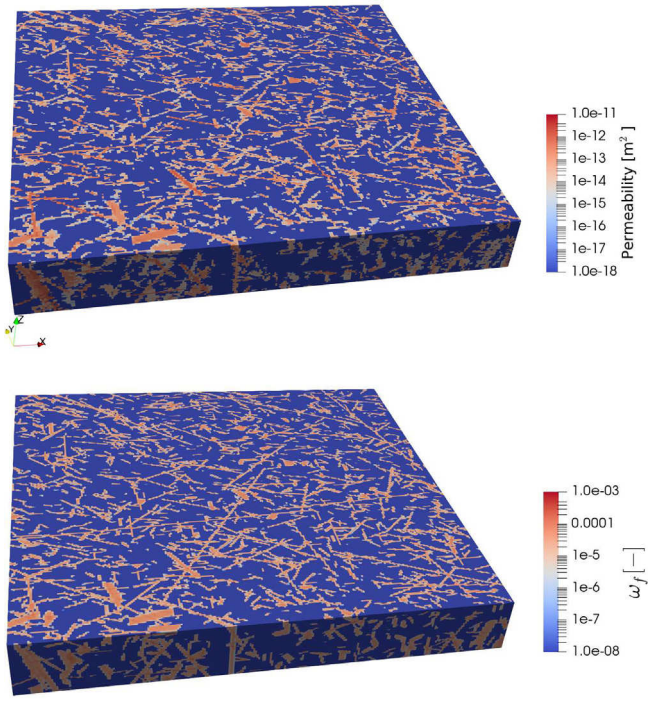

Fig. 8. Test Case #2 (TC2): DFN-derived (top) permeability and (bottom) fracture volume fraction of the Test Case #2 model.

The domain is a rectangular parallelepiped with the opposite vertices located at (0.0;0.0;-128.0) and (1024.0;1024.0;0.0), which is discretised with regular grid cells of size $\Delta_x = \Delta_y = 4$ m and $\Delta_z = 2$ m (i.e. 4,194,304 grid cells). Continuum DFN-derived parameters (fracture volume fraction and permeability) were calculated using the approach described by Svensson (2001). The resulting distributions of permeability and fracture volume fraction are shown in Fig. 8. Cells not intersected by any fracture were deactivated during the flow and transport calculation. The total number of active cells is 1,780,414.

Constant hydraulic pressure was applied to two narrow regions of width 10 m in the x-direction and length 1,024 m in the y-direction. Both regions are located at the top face at, x = 0 m (p_{in}) and x = 1,014 m (p_{out}), respectively, and a pressure difference $p_{in} - p_{out} = 1000$ Pa was prescribed. The rest of the boundaries were considered as no-flow boundaries.

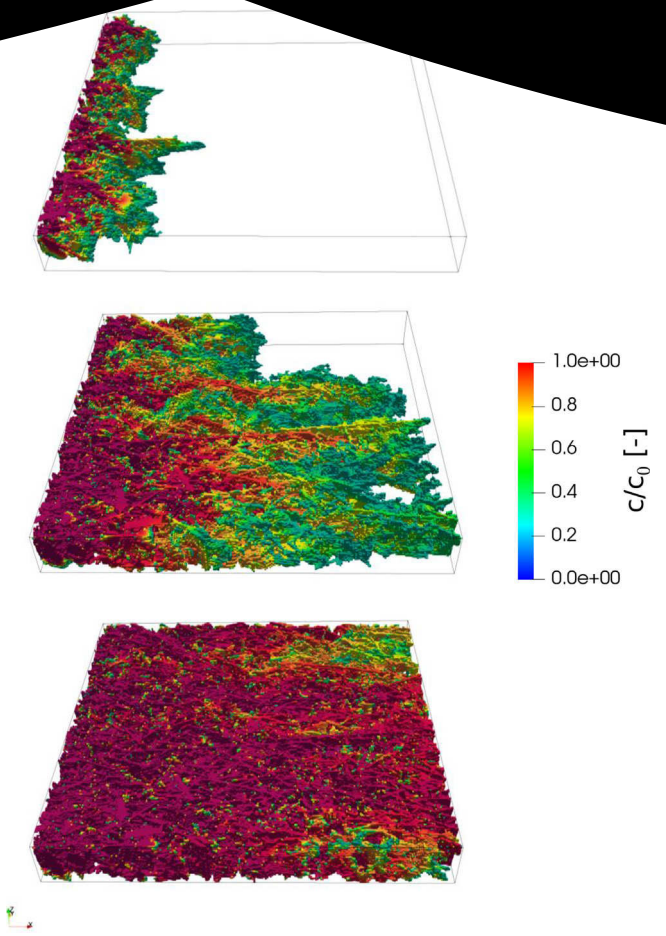

Fig. 9. TC2: concentration of the conservative tracer at time (a) 5 y, (b) 35 y and (c) 100 y. A portion of the domain is hidden in order to show a vertical cross-sections. Concentration values are normalised by the concentration in the boundary water. The cells with concentration $c/c_0 < 0.2$ are not shown.

^{4}He free water was assumed to infiltrate through the inlet boundary. ^{4}He production in the rock matrix is the same as used in TC1 (i.e. $G = 1.2 \cdot 10^{-10}$ mol/(m^3 y)). To keep track of conservative transport patterns, a conservative tracer was also added to the infiltrating boundary water.

Snapshots of the inert tracer concentration, taken at simulation time 5, 35 and 100 y are shown in Fig. 9. As already discussed in the previous test case, the analysis of the transient evolution of the conservative tracer is only used for a visual evaluation of groundwater flow patterns, as matrix diffusion processes are not included. At early times the tracer infiltrates through the most conductive fractures and after 100 y has already reached the discharge area, although less connected regions are still characterised by moderate to low concentrations.

The calculation was run in the JURECA booster module using 680 cores (~5200 transport degrees of freedom per process, as groundwater age is also included as primary species; the total number of transport degrees of freedom is given by the number of primary species multiplied by the number of active grid cells) and around 16,000 h of supercomputing time (i.e. ~24 h of wall clock time). The simulation was run out to 10,000 y in time to obtain steady-state concentration distributions of ^{4}He (Fig. 10). A few grid cells (51,811 cells; i.e. 2.9% of the total active cells) are poorly connected or even completely unconnected from the rest of the active cells. These cells, which have a very low fracture volume fraction and thus are expected to have minor impact on helium levels in the transmissive fractures, are not considered in the analysis discussed hereafter. ^{4}He levels show a qualitatively similar (but inverse) pattern as the conservative tracer: highly

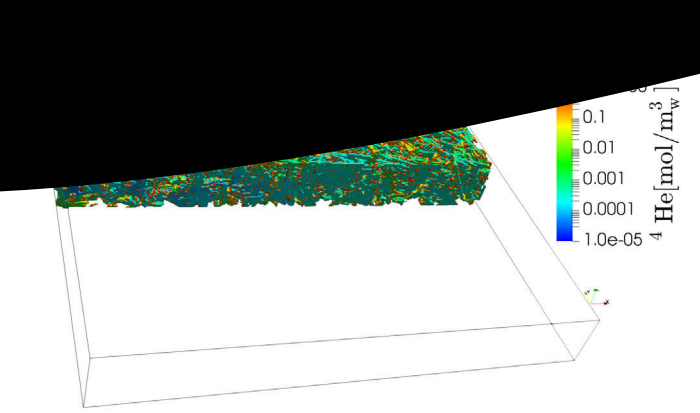

Fig. 10. TC2: concentration of ^{4}He at steady state. A portion of the domain is hidden in order to show a vertical cross-section. The cross section is the same as shown in Fig. 11.

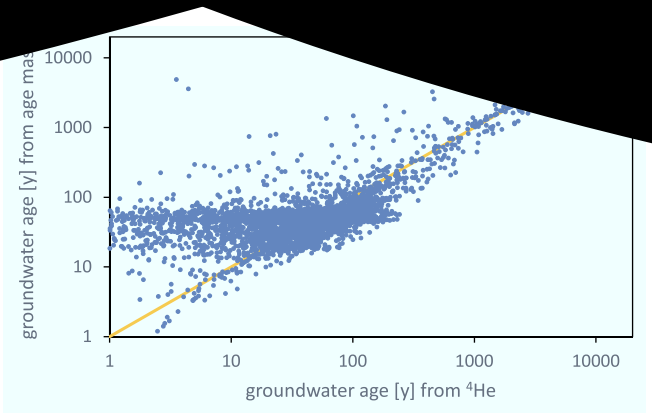

Fig. 12. TC2: scatter plot showing groundwater age computed using ^{4}He data and Eq. (17) vs. groundwater age computed using the concept of groundwater age mass (Goode, 1996) for all the grid cells located in a cross section taken at y = 512 m (i.e. same cross section of Fig. 11).

transmissive and connected fractures are clearly delineated by low ^{4}He concentration values, even far from the inlet boundary, indicating fast infiltration processes, whereas less connected regions are characterised by high ^{4}He concentration values ($[^4\text{He}] \cong 1\ \text{mol/m}^3_w$).

For the sake of simplicity, ^{4}He concentration levels are further analysed in a single vertical cross section, taken at $x = 512$ m and with normal vector parallel to the y-direction. Groundwater age was computed in this cross section using ^{4}He concentration values along with Eq. (17) (Fig. 11 top). Groundwater age was also computed using the concept of groundwater age mass (Goode, 1996) and the results are shown in Fig. 11 bottom.

It is worthwhile noting that the assumptions used to derive Eq. (17) (e.g. closed piston-like system with constant source of helium per unit of water in the flowing fractures) are clearly not fulfilled in this more realistic test case. Thus, comparing results obtained with Eq. (17) with results obtained with a less restrictive dating technique (Goode, 1996) should be seen as an assessment of the performance of the proposed methodology when applied to date groundwater in realistic complex environments.

The visual comparison between the two figures shows that the two methods provide qualitatively consistent estimates of groundwater age, with relatively young ages (<50 y) observed in the most conductive and connected fractures and with old ages observed in the less connected and mostly stagnant regions. A scatter plot showing groundwater age computed along the selected vertical cross section using ^{4}He data vs. groundwater age mass concept is also shown in Fig. 12. As already discussed in TC1, there are differences between the two estimates. Estimates obtained with Eq. (17) are not continuous and, in a number of points, significantly lower values of groundwater age are obtained. This difference is attributable to the strong contrasts in porosity of this model. In fact, these points are all located in the fringe of flowing fractures and have a significantly lower porosity. On the contrary, in the "core" of fractured zones, estimates obtained with the concept of groundwater age mass are generally lower due to the already discussed effect of dispersive fluxes of groundwater age, which tend to limit the maximum ages (Goode, 1996).

5. Discussion

The paper's main contribution is to present an analytical solution that, combined with available measurements of ^{4}He concentration, can provide first-order estimations of groundwater age in fractured aquifers. The method decouples the influence of matrix diffusion processes from the transport equation in the fracture under the assumption of steady-state conditions and, thus, gives estimates of groundwater age that are related to the groundwater velocity in the flowing fractures.

The main underlying assumption is that the medium behaves as a closed system, meaning that mixing at fracture intersections is neglected. Despite their high complexity and heterogeneity, evidence of flow being channelised along sparse channel networks have been observed in several laboratory and field experiments carried out in fractured media (e.g. Tsang and Neretnieks, 1998).

Another important assumption of Eq. (17) is that helium sources in the fracture, due to back-diffusion from the matrix, are constant along the considered pathways. This implies that helium production rate in the rock matrix (F), matrix porosity (ϕ) and fracture volume fraction (ω_f) are also constant. If we take the Forsmark site as an example, it has been shown that the first and second terms are relatively constant in the whole investigated domain (Drake et al., 2006; Trinchero et al., 2014). However, at the Forsmark site fracture intensity, which is related to the value of ω_f, decreases with depth. Thus, depending on the depth of the investigated domain, biases in the results could be introduced by the assumption of homogeneous production.

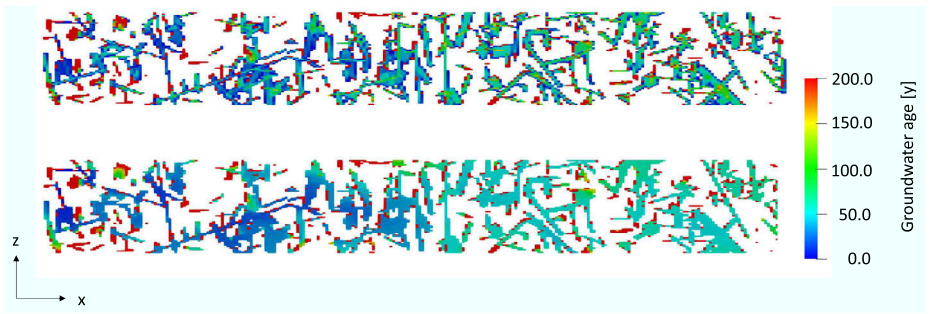

Fig. 11. TC2: cross section taken at y = 512 m showing (top) groundwater age computed using ^{4}He data and Eq. (17) and (bottom) groundwater age computed using the concept of groundwater age mass (Goode, 1996). Maximum values of groundwater age are here truncated to 200 y.

is constant
formulation δ_m im-
the spatial distribution of fracture volume
This hypothesis implies that a no-flux boundary is placed at $z = \delta_m$ (see Eq. (6c)), which implicitly means that the medium is conceptualised as a symmetric system of parallel fractures. This gross simplification of the fractured medium is commonly employed in contaminant transport simulations; see e.g. Sudicky and Frind (1982), Mahmoudzadeh et al. (2013), Cvetkovic (2017).

Advection is assumed to be the main transport mechanism in the flowing fractures. Therefore, the proposed method is suited to date groundwater age in relatively shallow and hydraulically active systems. For instance, Trinchero et al. (2014) assessed helium levels at Forsmark, Laxemar and Olkiluoto. The focus of that work was to understand helium transport patters at greater depth (from 200 to 1,000 meters below sea level). In those conditions, where diffusion becomes the main transport mechanism, the analytical solution (Eq. (17)) is clearly not applicable.

Finally, as already discussed above, the method presumes that steady-state conditions are attained. This is an import limitation in sites that have experienced strong changes in the hydrogeological regime over the past thousands of years due to e.g. landscape evolution or glaciation/de-glaciation events. Considering as starting point a hypothetical flushing event, interfacial ^{4}He fluxes will start increasing until reaching the steady state level of Eq. (6e). The time until steady-state ^{4}He fluxes are attained depends on the hydrodynamic conditions (i.e. groundwater velocity) and the distance from the recharge boundary. Moreover, increasing production rate, increasing porosity or decreasing fracture volume fraction would lead to an extended transient time frame.

In the second part of the paper we have presented a continuum-based formulation for the assessment of helium levels. The objective of the formulation is twofold: (i) to further validate the proposed analytical solution and (ii) to offer a computationally appealing approach for the investigation of steady-state helium levels using a stochastic continuum model (Iraola et al., 2019). In the formulation it is implicitly assumed that all the produced radiogenic helium is dissolved in the groundwater and this could lead to helium concentrations exceeding the solubility limit, particularly in poorly connected regions. Thus, the possibility of generation of gas bubbles should be considered, particularly at shallow depths where water pressure is relatively low.

6. Summary and conclusion

In porous aquifers, ^{4}He, which is produced by the alpha decay of natural uranium and thorium within the aquifer solids, has long been used to date groundwater age. The so-called linear accumulation method establishes a linear relationship between groundwater age and ^{4}He concentration, being the ratio between aquifer porosity and ^{4}He production rate the proportionality constant.

In fractured granitic rock, ^{4}He production takes place in the rock matrix and this leads to back-diffusion of ^{4}He from the matrix to the flowing fractures. We have analysed here the differential equations that govern ^{4}He production, diffusion and migration in a dual porosity system. At steady state, ^{4}He fracture/matrix interfacial surface flux is constant and equal to the bulk production rate scaled by the available size of the matrix. It turns out that a similar linear relationship between groundwater age and ^{4}He concentration can be established, being in this case the inverse of the bulk production rate scaled by the fracture volume fraction as the proportionality constant. This scaling factor provides a direct link with the underlying mass exchange processes.

The proposed solution, which has been validated using a single fracture-matrix verification test, can be readily applied to date groundwater age in shallow fractured systems where advection along
fractures is an importa
data, the method requires the knowledge
of the fractured rock system; namely the average fra
matrix size. Moreover, uranium and thorium content along with
porosity are needed to infer the bulk ^{4}He production rate, whereas the steady state solution does not depend on matrix diffusivity.

A continuum-based formulation, based on an Equivalent Continuous Porous (ECPM) medium, derived from an underlying Discrete Fracture Network (DFN), has also been presented and used to further analyse the applicability of the proposed dating framework. A simple and a more complex and realistic test case have been used to simulate steady-state ^{4}He levels and to derive related groundwater ages. Estimates of groundwater age based on the concept of groundwater age mass have also bee computed. The results obtained with the two different methodologies were in qualitatively good agreement. Discrepancies, and in particular generally higher groundwater estimates obtained from ^{4}He data, are due to the different underlying assumptions. The general conclusion of the verification tests, in particular TC2, is that the proposed dating methodology can provide reasonable estimates of groundwater age even in realistic fractured systems as long as flow is characterised by channelised pathways.

Declaration of Competing Interest

The authors declare no conflict of interest.

Acknowledgements

PT and MS thank the Swedish Nuclear Fuel and Waste Management Company (SKB) for the financial support. The authors gratefully acknowledge the computing time granted through JARA-HPC on the supercomputer JURECA at Forschungszentrum Jülich. The authors also want to thank Dr. Felipe de Barros and two anonymous reviewers for their very helpful comments.

References

Ballentine, C., Burnard, P., 2002. Production, release and transport of noble gases in the continental crust. Rev. Mineral. Geochem. 47, 481.

Bentley, H.W., Phillips, F.M., Davis, S.N., Habermehl, M.A., Airey, P.L., Calf, G.E., Elmore, D., Gove, H.E., Torgersen, T., 1986. Chlorine 36 dating of very old groundwater: 1. The Great Artesian Basin, Australia. Water Resour. Res. 22, 1991–2001. https://doi.org/10.1029/WR022i013p01991.

Bethke, C.M., Johnson, T.M., 2008. Groundwater age and groundwater age dating. Annu. Rev. Earth Planet. Sci. 36, 121–152.

Bethke, C.M., Zhao, X., Torgersen, T., 1999. Groundwater flow and the 4He distribution in the Great Artesian Basin of Australia. J. Geophys. Res. 104, 12999–13011.

Burgess, W.G., Hoque, M.A., Michael, H.A., Voss, C.I., Breit, G.N., Ahmed, K.M., 2010. Vulnerability of deep groundwater in the bengal aquifer system to contamination by arsenic. Nat. Geosci. 3, 83. https://doi.org/10.1038/ngeo750.

Clark, I.D., Fritz, P., 2013. Environmental Isotopes in Hydrogeology. CRC Press.

Cornaton, F., Park, Y.J., Deleersnijder, E., 2011. On the biases affecting water ages inferred from isotopic data. J. Hydrol. 410, 217–225. https://doi.org/10.1016/j.jhydrol.2011.09.024.

Cvetkovic, V., 2017. Statistical formulation of generalized tracer retention in fractured rock. Water Resour. Res. 53, 8736–8759.

Davis, S.N., Bentley, H.W., 1982. Dating groundwater: a short review. In: In nuclear and chemical dating techniques. Interpreting the environmental record. American Chemical Society Symposium Series.

Drake, H., Sandström, B., Tullborg, E., 2006. Mineralogy and Geochemistry of Rocks and Fracture Fillings from Forsmark and Oskarshamn: Compilation of Data for SR-Can (R-06-109). Svensk Kärnbränslehantering AB (SKB), Stockholm, Sweden.

Eichinger, F., Waber, H., Smellie, J., 2006. Characterisation of matrix pore water at the Okiluoto Investigation site, Finland . Posiva Oy, – Posiva 2006-103.

Goode, D.J., 1996. Direct simulation of groundwater age. Water Resour. Res. 32, 289–296.

Hadgu, T., Karra, S., Kalinina, E., Makedonska, N., Hyman, J.D., Klise, K., Viswanathan, H.S., Wang, Y., 2017. A comparative study of discrete fracture network and equivalent continuum models for simulating flow and transport in the far field of a hypothetical nuclear waste repository in crystalline host rock. J. Hydrol. 553, 59–70.

Hammond, G., Lichtner, P., Mills, R., 2014. Evaluating the performance of parallel subsurface simulators: an illustrative example with PFLOTRAN. Water Resour. Res. 50, 208–228.

Han, D., Kohfahl, C., Song, X., Xiao, G., Yang, J., 2011. Geochemical and isotopic

...ontinuum method
...sci. 130, 11–19. https://doi.org/
...g Centre, 2018. JURECA: modular supercomputer at Jülich supercomputing centre. J. Large-scale Res. Facil. 4. https://doi.org/10.17815/jlsrf-4-121-1.
Lichtner, P., Hammond, G.E., Lu, C., Karra, S., Bisht, G., Andre, B., Mills, R., Kumar, J., 2013. PFLOTRAN User Manual .
Mahmoudzadeh, B., Liu, L., Moreno, L., Neretnieks, I., 2013. Solute transport in fractured rocks with stagnant water zone and rock matrix composed of different geological layers-model development and simulations. Water Resour. Res. 49, 1709–1727.
Meinardi, C., Beusen, A., Bollen, M., Klepper, O., Willems, W., 1995. Vulnerability to diffuse pollution and average nitrate contamination of european soils and groundwater. Water Sci. Technol. 31, 159–165.
Molson, J., Frind, E., 2012. On the use of mean groundwater age, life expectancy and capture probability for defining aquifer vulnerability and time-of-travel zones for source water protection. J. Contam. Hydrol. 127, 76–87.
Neretnieks, I., 1981. Age dating of groundwater in fissured rock: influence of water volume in micropores. Water Resour. Res. 17, 421–422.
Neretnieks, I., 2013. Some aspects of release and transport of gases in deep granitic rocks: possible implications for nuclear waste repositories. Hydrogeol. J. 21, 1701–1716.
Neuman, S., 1988. A Proposed Conceptual Framework and Methodology for Investigating Flow and Transport in Swedish Crystalline Rocks (AR 88–37). Svensk Kärnbränslehantering AB (SKB), Stockholm, Sweden.
Reilly, T.E., Plummer, L.N., Phillips, P.J., Busenberg, E., 1994. The use of simulation and multiple environmental tracers to quantify groundwater flow in a shallow aquifer. Water Resour. Res. 30, 421–433.
Sanford, W.E., 1997. Correcting for diffusion in carbon-14 dating of ground water. Groundwater 35, 357–361.
Selroos, J.O., Walker, D.D., Ström, A., Gylling, B., Follin, S., 2002. Comparison of alternative modelling approaches for groundwater flow in fractured rock. J. Hydrol. 257, 174–188. https://doi.org/10.1016/S0022-1694(01)00551-0.
SKB, 2011. Long-term Safety for the Final Repository for Spent Nuclear Fuel at Forsmark: Main Report of the SR-site Project (TR-11-01). Svensk Kärnbränslehantering AB, Stockholm, Sweden.
...E., Frind, E., 1981. Carbon 14 da...
...plications of aquitard diffusion. Water Resour...
Sudicky, E.A., Frind, E., 1982. Contaminant transport in ...tical solution for a system of parallel fractures. Water Resour. Re...
Svensson, U., 2001. A continuum representation of fracture networks. Part I: ...basic test cases. J. Hydrol. 250, 170–186.
Svensson, U., 2001. A continuum representation of fracture networks. Part II: application to the Äspö hard rock laboratory. J. Hydrol. 250, 187–205.
Svensson, U., Ferry, M., 2014. Darcytools: a computer code for hydrogeological analysis of nuclear waste repositories in fractured rock. J. Appl. Math. Phys. 2, 365.
Svensson, U., Follin, S., 2010. Groundwater Flow Modelling of the Excavation and Operational Phases-Forsmark (R-09-19). Svensk Kärnbränslehantering AB, Stockholm, Sweden.
Torgersen, T., 1980. Controls on pore-fluid concentration of 4He and 222Rn and the calculation of 4He/222Rn ages. J. Geochem. Explor. 13, 57–75.
Torgersen, T., Clarke, W., 1985. Helium accumulation in groundwater, I: an evaluation of sources and the continental flux of crustal 4He in the Great Artesian Basin, Australia. Geochim. Cosmochim. Acta 49, 1211–1218.
Torgersen, T., Habermehl, M., Phillips, F., Elmore, D., Kubik, P., Jones, G.B., Hemmick, T., Gove, H.E., 1991. Chlorine 36 dating of very old groundwater: 3. Further studies in the Great Artesian Basin, Australia. Water Resour. Res. 27, 3201–3213.
Trinchero, P., Delos, A., Molinero, J., Dentz, M., Pitkänen, P., 2014. Understanding and modelling dissolved gas transport in the bedrock of three Fennoscandian sites. J. Hydrol. 512, 506–517.
Trinchero, P., Puigdomenech, I., Molinero, J., Ebrahimi, H., Gylling, B., Svensson, U., Bosbach, D., Deissmann, G., 2017. Continuum-based DFN-consistent numerical framework for the simulation of oxygen infiltration into fractured crystalline rocks. J. Contam. Hydrol. 200, 60–69. https://doi.org/10.1016/j.jconhyd.2017.04.001.
Tsang, C.F., Neretnieks, I., 1998. Flow channeling in heterogeneous fractured rocks. Rev. Geophys. 36, 275–298.
Varni, M., Carrera, J., 1998. Simulation of groundwater age distributions. Water Resour. Res. 34, 3271–3281.
Vidstrand, P., Rhén, I., Zugec, N., 2010. Groundwater Flow Modelling of Periods with Periglacial and Glacial Climate Conditions – Laxemar (Technical Report R-09-25). Svensk Kärnbränslehantering AB (SKB), Stockholm, Sweden.
Witherspoon, P.A., Wang, J.S., Iwai, K., Gale, J.E., 1980. Validity of cubic law for fluid flow in a deformable rock fracture. Water Resour. Res. 16, 1016–1024.